https://doi.org/10.5194/bg-2023-54
Preprint. Discussion started: 20 March 2023

Biogeosciences Discussions

North Atlantic patterns of primary production and phenology in two Earth System Models.

Jenny Hieronymus[1], Magnus Hieronymus[1], Matthias Gröger[2], Jörg Schwinger[3], Raffaele Bernadello[4], Etienne Tourigny[4], Valentina Sicardi[4], Itzel Ruvalcaba Baroni[1], Klaus Wyser[1]

[1]Swedish Meteorological and Hydrological Institute, SMHI, Norrköping, 601 76, Sweden
[2]Department of Physical Oceanography and Instrumentation, Leibniz Institute for Baltic Sea Research Warnemünde, Rostock, D-18119, Germany
[3]NORCE Climate & Environment, Bjerknes Centre for Climate Research, Bergen, 5007, Norway
[4]Barcelona Supercomputing Center, BSC, Barcelona, 08034, Spain

Correspondence to: Jenny Hieronymus (jenny.hieronymus@smhi.se)

Abstract. Uniquely long datasets, spanning 1750-2100, of daily output from two fully coupled CMIP6 Earth System Models, EC-Earth3-CC and NorESM2-LM, have been used to investigate the historical and future (under SSP5-8.5 scenario) evolution of marine net primary production and its phenology in a North Atlantic region (30-60° N). We compared the data to estimates of net primary production (NPP) derived from the CAFE satellite data and found significant differences between the Earth System Model simulations and the CAFE model. The low spatial resolution of the earth system models can explain much of such difference. However, the two models well represent both the magnitude of NPP and the seasonal cycles. The daily output made it possible to detect change points in peak NPP. Two major change points in peak NPP, of an amplitude not present in the PI-Control or the historical simulation, were detected in both Earth System Models in the first decade of the 21st century. The results clearly indicate a shift towards an earlier peak NPP with a clear inflection point in the beginning of the 21st century, at the end of the historical simulation. The early timing of the detected shifts in both models suggests that similar shifts could already have been initiated or start in the near future. This highlights the need for long term monitoring campaigns in the North Atlantic.

1 Introduction

Net Primary Production (NPP) is the rate of photosynthetic carbon fixation. In the ocean, primary production is performed by microscopic planktonic phototrophs with a turnover time of about one week. Though the individual plankton are small, the total marine primary production almost equals its terrestrial counterpart with an estimated size of marine NPP on the order of 50GtC/yr (eg. Kulk et al., 2020, Westberry et al., 2008, Silsbe et al., 2016, Carr et al., 2006). NPP constitutes the basis of the food chain and provides the energy for higher trophic levels. Changes in NPP thus affect the entire ecosystem and ultimately fisheries and human food supply (Stock et al., 2017). In addition, primary production is the first step in the biological carbon pump, a set of processes by which carbon is exported from the surface to the deep ocean through the

https://doi.org/10.5194/bg-2023-54
Preprint. Discussion started: 20 March 2023

sinking of organic matter. Understanding how the primary production and the subsequent export of organic carbon from the euphotic zone will change in future climate is thus vital for evaluating future uptake of atmospheric carbon dioxide (Honjo et al., 2014).

The north Atlantic is a region of particular importance for carbon sequestration in the deep ocean (Goris et al. 2018; Baker et al., 2022). This region contributes about 0.55-1.94 GtC/yr (Sanders et al. 2014) to the global export production, estimated to be 4-12 GtC/yr (de Vries and Weber, 2017). Moreover, here, cold water increases CO2 solubility and deep mixing and subduction in the subpolar portion of this area result in a net transport of carbon to depth, a combination of processes known as the solubility carbon pump.

NPP is affected by climate variability through precipitation, wind patterns, temperature and light and is thus projected to change with anthropogenic climate change. Though an increase in temperature may enhance the growth rate of phytoplankton and thereby the primary production, global NPP is projected to decrease (Behrenfeld et al., 2006; Steinacher et al., 2010; Bopp et al., 2013) though the uncertainty displayed in state-of-the-art Earth system Models (ESMs) is very large (Kwiatkowski et al., 2020). A projected NPP decline is often explained as being caused by increased water column stability that decreases the amount of nutrients available for primary production (Behrenfeld et al., 2006; Steinacher et al., 2010) but processes such as retreat of sea ice and increased stratification in high latitudes reduces the light limitation leading to NPP increases (Kwiatkowski et al., 2020).

Efforts have been made to estimate how NPP has already changed in the historical satellite record but the limited range of satellite time-series makes such endeavors difficult. Estimates range from -2.1% per decade over the period 1998-2015 (Gregg and Rousseaux, 2019) to no significant change (Kulk et al., 2020).

Apart from changes in total NPP, changes in seasonality and the timing of algae blooms can occur along with climate change with cascading effects into higher trophic levels up to fisheries and marine mammals. Depending on the onset of thermal stratification, the spring bloom may start earlier in the year causing a shift that may change the functioning and phenology of the entire ecosystem (Yamaguchi et al., 2022). Changes in the phenology, or the timing of recurring biological events, of phytoplankton blooms due to climate change have already been observed in the North Sea with the Continuous Plankton Recorder (CPR) since 1960, with data displaying a significantly earlier onset of the spring bloom (Chivers et al. 2020). A phenological change in phytoplankton blooms will affect zooplankton and larvae as the timing of available food resources will change, an effect known as the match/mismatch hypothesis (Cushing, 1990, Durant et al., 2007).

Henson et al. (2013) used historical simulations from six ESMs covering the years 1985-2009 and a high emission future scenario (RCP8.5) to study changes in the primary production phenology. They found a shift towards an earlier peak NPP

https://doi.org/10.5194/bg-2023-54
Preprint. Discussion started: 20 March 2023

for most areas around the globe. However, the monthly resolution of the CMIP5 data dampens the phenology signal considerably. In a more recent study, Henson et al. (2018) used higher frequency model output to investigate the effect of temporal resolution on results of phytoplankton phenology. They found that in order to detect long term trends in bloom timing, a maximum temporal resolution of not more than 20 days is required.

However, even though a 20-day resolution may be adequate to detect long term trends, it is certainly not enough for detecting the timing of a rapid change in phenology in the course of global warming. In this paper, we use a uniquely long time series of daily output from two ESMs that contributed to the 6th Coupled Model Intercomparison Project (Eyring et al., 2016), to investigate the evolution of oceanic primary production and its phenology in a region 30-60^{o} N, 67^{o} W-9^{o}E in the North Atlantic in the period 1750-2100. We investigate the occurrence of major changes in the time-series of the day of peak NPP using change point analysis.

2 Method

Daily output of vertically integrated primary production has been produced using NorESM2-LM and EC-Earth3-CC for 100 years pi-control, historical (1850-2014) and the high emission scenario SSP5-8.5 (2015-2100, Kriegler et al., 2017). All runs are forced with prescribed atmospheric CO2 concentrations (concentration driven) in accordance with Meinshausen et al., 2020. The models are described in section 2.1. Section 2.2 describes the observational data set and section 2.3 provides an overview of the change point analysis method used.

2.1 Models

2.1.1 EC-Earth3-CC

EC-Earth3 is an ESM developed by a European consortium of institutes and universities (Döscher et al. 2022). It is available in several different configurations. For this work, we have used EC-Earth3-CC which consists of the Integrated Forecast System (IFS) CY36R4 of the European Centre for Medium-Range Weather Forecasts (ECMWF) for simulating physics of the atmosphere and land surface, Nemo3.6 (Madec, 2015) for ocean physics, LPJ-Guess (Smith et al., 2014) for terrestrial vegetation and PISCES (Aumont et al., 2015) for ocean biogeochemistry. In concentration driven form, PISCES is fed a spatially uniform atmospheric pCO2 while a CO2 mapping occurs within IFS to account for regional heterogeneities.

PISCES is a mixed Monod-quota model simulating two different phytoplankton functional types, diatoms and nanophytoplankton, two size classes of zoo-plankton, micro and meso, and nutrients nitrate, ammonium, phosphate, iron and silicate. Iron and silicate are modeled using quotas in phytoplankton and the other nutrients with fixed Redfield ratios. Phytoplankton growth depends on the external concentration in nutrients, light and temperature. PISCES is suited for a wide range of spatial and temporal scales, including quasi-steady state simulations on the global scale. PISCES further simulates

https://doi.org/10.5194/bg-2023-54
Preprint. Discussion started: 20 March 2023

the carbon system, as well as dissolved and particulate organic matter. Primary production is the growth of phytoplankton thus the term excludes mortality, excretion and grazing. The integrated primary productivity used for the analysis is integrated over the water column and also summed over the two different phytoplankton functional types.

PISCES has been used and validated in a number of settings (Ramirez-romero et al., 2020; Gutknecht et al., 2019; Kwiatkowski et al., 2018). Skyllas et al. (2019) validated EC-Earth3, in an offline ocean only NEMO-PISCES version, for the North-west Atlantic using cruise data of temperature, salinity and nutrients and chlorophyll-a and found a good agreement with observations. Primary production has not previously been validated for EC-Earth3-CC although the air-sea CO2 flux, which is strongly affected by primary production, was compared to an observation based climatology in Döscher et al. (2022). Their results showed stronger uptake of CO2 than observations in the North Atlantic, thought to be caused by too active convection in the Labrador Sea.

2.1.2 NorESM2-LM

The Norwegian Earth System Model NorESM2 (Seland et al., 2020, Tjiputra et al, 2020) is a fully coupled ESM, which is based on the Community Earth System Model version 2 (CESM2, Danabasoglu et al. 2020) but employs a different ocean component (the Bergen Layered Ocean Model, BLOM) and a modified atmosphere model (CAM6-Nor). The land surface and terrestrial biogeochemistry is represented by the Community Land Model version 5 (CLM5). BLOM uses isopycnic coordinates in the vertical (below a bulk mixed layer represented by two non-isopycnic model layers on top) and it includes the iHAMOCC model to represent ocean biogeochemistry. BLOM is coupled to the sea-ice component CICE5, which is the same as in CESM2. The LM version of NorESM2 used in this study has an atmosphere-land resolution of 2° and a nominal ocean model resolution of 1°. iHAMOCC is derived from the HAMOCC model (Six and Maier-Reimer, 1996; Ilyina et al. 2013) and was adapted for the use with isopycnic coordinates by Assman et al.(2010). HAMOCC includes a relatively simple NPZD ecosystem model with one phytoplankton and one zooplankton compartment and an implicit representation of calcifying and silicifying organisms. The model simulates nitrogen and phosphorus nutrients as well as dissolved iron with phytoplankton nutrient uptake according to Redfield molar ratios.

NorESM2-LM has been validated with regards to biogeochemical variables including primary production in Tjiputra et al. (2020). The results show a seasonal cycle of marine NPP that is reasonably well captured in amplitude but with a too low annual mean.

2.2 Observations

Direct observational data records of primary production are scarce and in order to validate the two ESMs with respect to NPP, we have chosen to use data from a satellite based approach. There are several different methods for deriving NPP

https://doi.org/10.5194/bg-2023-54
Preprint. Discussion started: 20 March 2023

estimates from satellite data. Often they are either based on ocean color (Behrenfeld and Falkowski, 1997), carbon (Westberry et al., 2008) or absorption (Smyth et al., 2005).

In this work, we use data from the Carbon, Absorption and Fluorescence Euphotic-resolving (CAFE) model (Silsbe et al. 2016), freely available through the Ocean Productivity site (http://sites.science.oregonstate.edu/ocean.productivity/index.php). The model utilizes satellite derived properties and has been shown to compare well to in situ observations (Johnson and Bif, 2021). We here utilize the Modis-aqua dataset from 2002 to 2021.

2.3 Change point analysis

Change point detection is a method to identify abrupt change in a time-series. In climate science, the method has been used to detect shifts in a wide variety of quantities (Beaulieu et al., 2012) such as AMOC strength (Smeed et al., 2018), coastal organic C sequestration (Watanabe et al., 2018), and cod stock (Möllmann et al., 2021). We have used change point detection to identify rapid change in the calendar-day of peak NPP. The calculations have been performed using the Python package Ruptures (Truong et al. 2020).

Change point detection requires a search method related to the number of change points, and a model related to the type of change. Many methods of change point analysis focus on finding a predetermined number of shifts in a predefined quantity, such as the time series mean or variance (Truong et al., 2020). We have chosen to use the Pelt search method developed by Killick et al. (2012). This method does not require the number of change points to be determined beforehand. Instead, a penalty is defined that is related to the amplitude of the change of interest. A small penalty generates many change points, which may arise due to intra-annual variability or noise, while a large penalty instead only gives the largest, if any, changes in the time series. By choosing a large enough penalty, the number of change points can in this way be tuned.

Furthermore, instead of predefining the type of time series change, we have chosen to use a kernel based non-parametric model developed by Arlot et al. (2013), in the following called “the kernel based model”. This model gives all changes in the probability distribution of the time-series; mean, variance and higher order changes such as skew and kurtosis. The upside of this approach is that no large changes are missed. The method does not, however, provide the information on which change point is related to what type of change. Therefore, we complement the method with the Least absolute deviation (l1) model that detects changes in the median and the Least squared deviation (l2) that detects changes in the mean of the time-series.

3 Results and discussion

3.1 Models vs observations

https://doi.org/10.5194/bg-2023-54
Preprint. Discussion started: 20 March 2023

We have compared the daily ESM data with 8 day averaged NPP estimates from the CAFE data (Silsbe et al, 2016). Seasonal mean NPP over the MODIS-aqua period 2003-2021, for March, April, May (MAM), June, July, August (JJA) and September, October, November (SON) seasons are shown in Fig. 1. The figure shows large spatial differences between CAFE, EC-Earth3-CC and NorESM data. Most notably, EC-Earth3-CC shows a very strong primary production in MAM over the gulf stream region. We also see a tendency for stronger primary production in this region in the CAFE data, although the enhanced production is much more confined. The high resolution CAFE data show that the enhanced production occurs in the warm Gulf stream eddies. The low resolution of the ESMs gives a wider and less constrained warm water transport as a result of unresolved eddies.

The NorESM results in the Gulf stream region are closer to the CAFE data, although the production in the northern part of the domain is underestimated in both ESMs. Both ESMs also fail to capture the strong JJA production in the northern part of the domain, between the Labrador current and the British Isles and do not represent the strong European coastal production seen in the CAFE data. For the the latter well compiled runoff nutrients and high resolution are required to represent coastal dynamics (Gröger et al., 2013; Sein et al., 2020).

Peak NPP over this period occurs in May in EC-Earth3-CC and in June in NorESM2-LM as can be seen in the seasonal cycle in Fig. 2. The figure shows the mean seasonal cycle over the period 2003-2021 taken over all grid points in the domain, along with standard deviations. Due to the smaller area seen by satellites in winter, the CAFE data contains missing data over the winter months. In order to correctly compare the seasonal cycles, the ESM data was masked by the area covered by CAFE data in Fig. 2.

The results indicate a reasonable agreement in the maximum and minimum size of primary production where EC-Earth3-CC is closer in magnitude and NorESM2-LM closer in timing. The CAFE data does, however, show a significantly longer season and the annual mean is therefore larger with 417 mgC m-2 day-1 compared to 359 mgC m-2 day-1 in EC-Earth3-CC and 228 mgC m-2 day-1 in NorESM2-LM. A notable feature in Fig. 2 is the skewed shape of the EC-Earth3-CC seasonal cycle. Where the observations and NorESM2-LM display a seasonality that appears almost normally distributed over the year with a peak in June, EC-Earth3-CC primary production is shifted towards the earlier part of the year. It should be noted that the higher resolution model version NorESM1-ME displayed a North Atlantic seasonal cycle of NPP similar to what is seen in EC-Earth3-CC (Tjiputra et al., 2020). Development targeting this behavior at high latitudes, with a too strong spring bloom and a too strong decline after the bloom, was performed in NorESM2 by generally increasing the grazing pressure during a bloom and by increasing the amount of nutrients incorporated into dissolved organic matter (Tjiputra et al., 2020).

https://doi.org/10.5194/bg-2023-54
Preprint. Discussion started: 20 March 2023

3.2 Historical and future primary production

The time-series of annual mean NPP from 100 years of pi-control, historical and SSP5-8.5 are shown in Fig. 3 for EC-Earth3-CC, NorESM2-LM along with the annual mean CAFE data for the period 2003-2021.

The figure reveals a large multidecadal variability in EC-Earth3-CC compared to NorESM2-LM. The Cafe data seems to display an even larger long term variability although the limited length of the timeseries makes comparisons of multidecadal variability problematic. The small interannual variability in NorESM2-LM also makes it easier to visually discern the declining trend in NPP over the later part of SSP5-8.5.

The seasonal cycle of primary production over historical and SSP5-8.5 (1850 to 2100) for the two models are shown in Fig. 4. Both models show a decline in primary production over SSP5-8.5 although the decline is concentrated around the time of the NPP peak in NorEMS2-LM while it is more pronounced and more equally distributed over the seasonal cycle in EC-Earth3-CC. Note, however, that the reduction in NPP in EC-Earth3-CC displayed in Fig 4. is not much larger than multidecadal NPP variability seen in earlier periods of the NPP time series (cf. Fig. 3) which makes it difficult to attribute the decline to climate change. Moreover, the figure reveals a shift in phenology towards an earlier peak NPP evident for both EC-Earth3-CC and NorESM2-LM.

In order to find how the shift in phenology is distributed over the region, the spatial distribution of the day of peak NPP averaged over the 30 year period 1850-1879 for the two ESMs is shown in Fig 5. Also shown in the figure is the difference of the ESM results averaged over the period 1970-1999 and 2070-2099 from the early period 1850-1879. In the early period, 1850-1879, EC-Earth3-CC displays a pattern of later bloom in the Labrador Sea compared to the rest of the domain, while NorESM2-LM has a later peak NPP south of Greenland and in the Gulf stream area compared to the rest of the domain. Both models show an earlier peak NPP in the southernmost part compared to the rest of the region.

The period 1970-1979 shows small and scattered differences from the early period. In the late period, 2070-2099, most of the domain experience an earlier peak NPP but with some notable exceptions. Parts of the Gulf stream region display a markedly later peak NPP in the NorESM2-LM data compared to the early period, 1850-1879. This corresponds to an expansion of the pattern of late peak NPP in the Gulf stream region seen in the early period. Averaged over the entire domain, peak NPP is

https://doi.org/10.5194/bg-2023-54
Preprint. Discussion started: 20 March 2023

only one day earlier in the period 2070-2099 (day 125) compared to 1850-1879 (day 126) in NorESM2-LM. The standard deviation of the mean difference between these two periods is, however, 30.7 days which underscores the heterogeneous pattern in the day peak NPP over the region.

In EC-Earth3-CC the pattern of earlier peak NPP is more robust over the domain but with the southernmost part displaying a later peak NPP in the late period, 2070-2099. The region corresponds to data points with very early peak NPP in the period 1850-1879. A notable feature is the much later bloom west of the Strait of Gibraltar. NPP in this region is greatly reduced in the late period compared to 1850-1879 caused by a strong reduction in winter surface nitrate concentration (not shown). The NPP seasonality in this area shifts from a clear spring peak to an extended period of weak NPP (not shown). The peak is therefore less well defined and located later in the year. Averaged over the entire domain, EC-Earth3-CC displays an earlier peak NPP by 10.7 days in the period 2070-2099 (day 109) compared to the early period (day 120) with a regional standard deviation of 32.8 days which is similar in magnitude to the standard deviation of 30.7 days in the NorESM2-LM results. The largest shifts towards earlier peak NPP are seen in the Labrador sea in EC-Earth3-CC and south of Greenland in NorESM2-LM.

The earlier bloom displayed in our results is in agreement with Asch et al. (2019) who showed that blooms north of 40°N shifted earlier under RCP8.5 using 5 daily output from GFDL ESM2M including the biogeochemical model TOPAZ2.0. In contrast, Henson et al. (2018) reports, using an ocean only model (MEDUSA-2.0, NEMO), a start of bloom shifting later in the year under RCP8.5 in most parts of the North Atlantic. However, both studies relate to surface chlorophyll and not NPP, which makes the comparison problematic. Moreover, our temporal resolution is higher and both Henson et al. (2018) and Asch et al. (2019) use the start of bloom as well as length of bloom as a phenological indicators instead of the timing of the annual peak which further complicates the comparison.

Averaging over the entire domain allows us to look at the mean phenology change of NPP. It also allows us to identify change points in the mean phenology. Fig. 6 shows the time-series of the day of peak NPP averaged over the entire region. The time-series shows a decline in the day of peak NPP for both models over the 21st century under SSP5-8.5 with the start of the decline occurring at the end of the historical simulation. Fig. 6 also displays the change-points of the time-series, found by the kernel based model, for three different choices of penalty, which is related to the amplitude of the probability

https://doi.org/10.5194/bg-2023-54
Preprint. Discussion started: 20 March 2023

distribution change. The largest penalty is tuned so that only one major change point is found. This generates the most important change point in the time-series. In EC-Earth3-CC this occurs in the year 2010 and in NorESM2-LM it instead occurs in 2070. Decreasing the penalty to find two change points generates a change point also in the year 2095 in the EC-Earth3-CC data and in the year 2007 in NorESM2-LM.

To shed some light on the type of change occurring at the identified times, we complement the analysis by using the l1 and l2 change point models that identify respectively changes in median and mean. We use the largest penalty such that the search method only picks up the most important change-point in the time-series. The results show that both models l1 and l2 identify the 2010 change point found by the kernel based model in the EC-Earth3-CC data, while neither l1 or l2 identifies the largest change point in NorESM2-LM found by the kernel based model. l1 comes closest to the 2070 change point in NorESM2-LM. The mean shift occurring first after the beginning of the 21st century is consistent with the results of Henson et al (2009), who found no long term trend in the subpolar north Atlantic towards earlier or later blooms in model data spanning 1959-2004. The day of peak NPP averaged over the 50 years before and after the 2010 change point reveals a reduction in the day of peak NPP of 12 days in EC-Earth3-CC and 10 days in NorESM2-LM. Importantly, a major change point occurs in both ESMs at the end of the historical simulation. A shift towards an earlier peak NPP thus occurs for both models before the onset of the future scenario simulation.

But how well do change points in the spatial mean of the region represent the separate grid points? The year during which the largest change point for every grid point occurs is shown in Fig. 7. The penalty has been tuned to catch only the single largest change point. The results broadly correspond to the results seen in the spatial mean time series with a major change point occurring after the year 2000. Few grid points display a change point earlier than that. Furthermore, EC-Earth3-CC displays an earlier major change point for most grid points as compared to NorESM2-LM. The northern part of the domain, i.e. regions where the euphotic zone is more vigorously coupled to the deep sea by vertical mixing like the Labrador Sea, northern North Atlantic and the sub-polar gyre, shows the earliest change point in the EC-Earth3-CC results close to the year 2000. The south eastern part of the domain displays the latest change point in both NorESM2-LM and EC-Earth3-CC.

The seasonal cycle of phytoplankton blooms has been explained with various theories. An often cited theory is the Critical Depth Hypothesis (Sverdrup, 1953) which postulates that a bloom can occur when the mixed layer has shoaled to a critical

https://doi.org/10.5194/bg-2023-54
Preprint. Discussion started: 20 March 2023

depth where the light limited gross production outweighs respiration. It does not, however, give an explanation as to when a bloom starts and ends. A more recent theory, termed the Disturbance Recovery Theory, of the timing of blooms was given by Behrenfeld (2010) (see also Behrenfeld and Boss, 2018). The theory suggests a balance between the growth and the loss in terms of respiration, grazing and disturbances to the physical environment such as the depth of the mixed layer. In Fig. 8 , we have plotted the first day of the year at which the spatial mean Mixed Layer Depth (MLD) shoals to 40m or less. The results show that, like the day of max NPP, the day of MLD above 40m occurs progressively earlier over SSP5-8.5 for both EC-Earth3-CC and NorESM2-LM. The most important change point in the day of MLD above 40m time-series found using the kernel based model, occurs in 2030 in EC-Earth3-CC and in 2031 in NorESM2-LM. However, allowing for two change points generates one change point in 1995 and one in 2045 for EC-Earth3-CC, and one in 2017 and one in 2061 for NorESM2-LM. Although the change points in the day of MLD above 40m are not directly corresponding to the change points found in the time series of the day of peak NPP (Fig. 6), the largest change points in the time series occur in the late historical simulation and in SSP5-8.5 for both models. The choice of 40m is somewhat arbitrary. We have however tested for change points on cut off depths between 25 and 80m with no difference to the results of the location of change points.

To elucidate on the correlation between the day of MLD above 40m and the day of max NPP, the cross correlation between the area averaged time-series shown in Figs. 6 and 7 has been plotted in Fig. 9. The figure shows a notable correlation, well above the 95% confidence bound, between the two indices for both ESMs. The maximum correlation occurs for zero lag, indicating, as expected, that peaks in these variables tend to occur within the same year. The clearly declining correlations with longer lags may reflect the low-frequency cycles controlled by the Atlantic multi-decadal variability which controls environmental parameters on time scales > 60 years (e.g. Börgel et al. 2020).

4 Summary and conclusions

Using uniquely long datasets of 350 years of daily output from two CMIP6 fully coupled ESMs, we have analyzed NPP for an area covering 30-60ºN, 67ºW-9ºE in the North Atlantic, with an emphasis on the phenology. We have compared the vertically integrated NPP for the two ESMs with the satellite based CAFE model. Both models show deviations from the CAFE data, partly due to unresolved eddies in the Gulf stream region. Averaged over the domain, the seasonal cycle of the CAFE data displays a longer season than the two ESMs, where NorESM2-LM better captures the timing of peak NPP and EC-Earth3-CC is closer in annual average NPP. The multi-decadal variability is smaller in NorESM2-LM than in EC-

https://doi.org/10.5194/bg-2023-54
Preprint. Discussion started: 20 March 2023

Earth3-CC. The CAFE data seem to show larger multidecadal variability than both ESMs though this is difficult to determine given the relatively short (2003-2021) satellite record.

The ESM data show that shifts in the seasonal cycle occur mainly during the 21st century with reduced NPP as well as a peak NPP occurring earlier in the year. The largest change in the day of peak NPP occurs in the north western part of the domain for both ESMs. Using change-point analysis, we have shown that the largest two change points in the area averaged day of peak NPP occurs after the year 2000 in both ESMs. The first of the two change points occurs in 2010 in EC-Earth3-CC and in 2007 in NorESM2-LM. One additional major change point was detected in 2070 in NorESM2-LM and 2090 in EC-Earth3-CC. We have also shown that the largest change point in the day of peak NPP occurring after the year 2000 is a robust feature even for individual grid points. Comparing the average of the last 30 years (2070-2099) to average over the period 1850-1879, the day of peak NPP is earlier by 1/11 day/s in NorESM2-LM/EC-Earth3-CC but with a regional standard deviation of 31/33 days respectively, high-lighting the heterogeneous regional pattern displayed in both ESMs. Furthermore, in similar to the change points in the day of peak NPP, the largest change points in the first day of MLD smaller or equal to 40m occur in the 21st century. Cross correlation shows significant correlation between this variable and the day of peak NPP.

Our results point to a phenological shift occurring in the early 21st century in the vertically integrated NPP in the North Atlantic (30^{o}-60^{o}N, 67^{o}W-9^{o}E). Shifts in the phenology may have an impact on fishery yields through the mismatch of fish spawning and available resources. Furthermore, carbon sequestration in this highly productive region may be affected by changes in ecosystem structure affecting the export production.

Code availability: The EC-Earth3 code is available from the EC-Earth development portal for members of the consortium. All code related to CMIP6 forcing is implemented in the component models. Model codes developed at ECMWF, including the atmosphere model IFS, are intellectual property of ECMWF and its member states. Permission to access the EC-Earth3 source code can be requested from the EC-Earth community via the EC-Earth website (http://www.ec-earth.org/, EC-Earth consortium, 2019a) and may be granted if a corresponding software license agreement is signed with ECMWF. The repository tag for the version of EC-Earth that is used in this work is 3.3.1. Currently, only European users can be granted access due to license limitations of the atmosphere model. The component models NEMO, LPJ-GUESS, TM5, and PISM are not limited by their licenses.

The NorESM code can be accessed via zenodo: Seland, Ø., Bentsen, M., Olivié, D., Toniazzo, T., Gjermundsen, A., Graff, L. S., Debernard, J. B., Gupta, A. K., He, Y., Kirkevåg, A., Schwinger, J., Tjiputra, J., Aas, K. S., Bethke, I., Fan, Y., Gao, S., Griesfeller, J., Grini, A., Guo, C., Ilicak, M., Karset, I. H. H., Landgren, O., Liakka, J., Moree, A., Moseid, K. O.,

335 Nummelin, A., Spensberger, C., Tang, H., Zhang, Z., Heinze, C., Iversen, T., and Schulz, M.: NorESM2 source code as used for CMIP6 simulations (includes additional experimental setups, extended model documentation, automated inputdata download, restructuring of BLOM/iHAMOCC input data), Zenodo [code], https://doi.org/10.5281/zenodo.3905091, 2020.

Data availability: The data used to produce the figures in this manuscript can be downloaded from
340 Zenodo:10.5281/zenodo.7716480

Author contribution: JH performed the EC-Earth3-CC model run, made the analysis with contributions from MH, and drafted the manuscript. MG contributed to the research design. JS performed the NorESM2-LM run. ET, RB and VS made the EC-Earth3-CC setup and contributed to the EC-Earth3-CC model run. IRB contributed to the writing of the paper. KW
345 assisted in setting up and running EC-Earth3-CC. All co-authors contributed to the writing of the paper.

Competing interests: The authors declare that they have no conflict of interest.

Disclaimer: The work reflects only the author's/authors' view; the European Commission and their executive agency are not
350 responsible for any use that may be made of the information the work contains.

Acknowledgements: This project has received funding from the European Union's Horizon 2020 research and innovation programme under grant agreement No 820989 (project COMFORT, Our common future ocean in the Earth system – quantifying coupled cycles of carbon, oxygen, and nutrients for determining and achieving safe operating spaces with respect
355 to tipping points). R. B. acknowledges support from the European Union's Horizon 2020 research and innovation programme under the Marie Skłodowska-Curie grant agreement No GA 708063 (NetNPPAO).

References

Arlot, S., Celisse, A. and Harchaoui, Z. (2012). A kernel multiple change-point algorithm via model selection. Preprint. Available at https://arxiv.org/abs/1202.3878v2.

360 Asch, R. G., Stock, C. A., & Sarmiento, J. L. (2019). Climate change impacts on mismatches between phytoplankton blooms and fish spawning phenology. Global Change Biology, 25(8), 2544–2559. https://doi.org/10.1111/gcb.14650

Assmann, K. M., Bentsen, M., Segschneider, J., and Heinze, C.: An isopycnic ocean carbon cycle model, Geosci. Model Dev., 3, 143–167, https://doi.org/10.5194/gmd-3-143-2010, 2010.

Aumont, O., Ethé, C., Tagliabue, A., Bopp, L., & Gehlen, M. (2015). PISCES-v2: An ocean biogeochemical model for carbon and ecosystem studies. *Geoscientific Model Development*, *8*(8), 2465–2513. https://doi.org/10.5194/gmd-8-2465-2015

Beaulieu Claudie, Chen Jie and Sarmiento Jorge L. (2012). Change-point analysis as a tool to detect abrupt climate variationsPhil. Trans. R. Soc. A. 370. 1228–1249. http://doi.org/10.1098/rsta.2011.0383

Behrenfeld, M. J., & Falkowski, P. G. (1997). Photosynthetic rates derived from satellite-based chlorophyll concentration. *Limnology and Oceanography*, *42*(1), 1–20. https://doi.org/10.4319/lo.1997.42.1.0001

Behrenfeld, M. J. (2010). Abandoning Sverdrup ' s Critical Depth Hypothesis on phytoplankton blooms. *Ecology*, *91*(4), 977–989.

Behrenfeld, M. J., O'Malley, R. T., Siegel, D. A., McClain, C. R., Sarmiento, J. L., Feldman, G. C., Milligan, A. J., Falkowski, P. G., Letelier, R. M., & Boss, E. S. (2006). Climate-driven trends in contemporary ocean productivity. *Nature*, *444*(7120), 752–755. https://doi.org/10.1038/nature05317

Behrenfeld, M. J., & Boss, E. S. (2018). Student's tutorial on bloom hypotheses in the context of phytoplankton annual cycles. *Global Change Biology*, *24*(1), 55–77. https://doi.org/10.1111/gcb.13858

Bopp, L., Resplandy, L., Orr, J. C., Doney, S. C., Dunne, J. P., Gehlen, M., Halloran, P., Heinze, C., Ilyina, T., Séférian, R., Tjiputra, J., & Vichi, M. (2013). Multiple stressors of ocean ecosystems in the 21st century: Projections with CMIP5 models. *Biogeosciences*, *10*(10), 6225–6245. https://doi.org/10.5194/bg-10-6225-2013

Börgel, F., C. Frauen, T. Neumann, and H. E. M. Meier., The Atlantic Multidecadal Oscillation controls the impact of the North Atlantic Oscillation on North European climate, Environmental Research Letters, https://doi.org/10.1088/1748-9326/aba925. 2020

Chivers, W. J., Edwards, M., & Hays, G. C. (2020). Phenological shuffling of major marine phytoplankton groups over the last six decades. *Diversity and Distributions*, *26*(5), 536–548. https://doi.org/10.1111/ddi.13028

Cushing, D. H. (1990). Plankton Production and Year-class Strength in Fish Populations: an Update of the Match/Mismatch Hypothesis. Advances in Marine Biology, 26, 249-293. https://doi.org/10.1016/S0065-2881(08)60202-3

Danabasoglu, G., Lamarque, J. F., Bacmeister, J., Bailey, D. A., DuVivier, A. K., Edwards, J., Emmons, L. K., Fasullo, J., Garcia, R., Gettelman, A., Hannay, C., Holland, M. M., Large, W. G., Lauritzen, P. H., Lawrence, D. M., Lenaerts, J. T. M., Lindsay, K., Lipscomb, W. H., Mills, M. J., … Strand, W. G. (2020). The Community Earth System Model Version 2 (CESM2). *Journal of Advances in Modeling Earth Systems*, *12*(2), 1–35. https://doi.org/10.1029/2019MS001916

Durant, J. M., Hjermann, D., Ottersen, G., & Stenseth, N. C. (2007). Climate and the match or mismatch between predator requirements and resource availability. *Climate Research*, *33*(3), 271–283. https://doi.org/10.3354/cr033271

Döscher, R., Acosta, M., Alessandri, A., Anthoni, P., Arsouze, T., Bergman, T., Bernardello, R., Boussetta, S., Caron, L.-P., Carver, G., Castrillo, M., Catalano, F., Cvijanovic, I., Davini, P., Dekker, E., Doblas-Reyes, F. J., Docquier, D., Echevarria, P., Fladrich, U., Fuentes-Franco, R., Gröger, M., v. Hardenberg, J., Hieronymus, J., Karami, M. P., Keskinen, J.-P., Koenigk, T., Makkonen, R., Massonnet, F., Ménégoz, M., Miller, P. A., Moreno-Chamarro, E., Nieradzik, L., van Noije, T., Nolan, P., O'Donnell, D., Ollinaho, P., van den Oord, G., Ortega, P., Prims, O. T., Ramos, A., Reerink, T., Rousset, C., Ruprich-Robert, Y., Le Sager, P., Schmith, T., Schrödner, R., Serva, F., Sicardi, V., Sloth Madsen, M., Smith, B., Tian, T., Tourigny, E., Uotila, P., Vancoppenolle, M., Wang, S., Wårlind, D., Willén, U., Wyser, K., Yang, S., Yepes-Arbós, X., and Zhang, Q.: The EC-Earth3 Earth system model for the Coupled Model Intercomparison Project 6, Geosci. Model Dev., 15, 2973–3020, https://doi.org/10.5194/gmd-15-2973-2022, 2022.

Gregg, W. W., & Rousseaux, C. S. (2019). Global ocean primary production trends in the modern ocean color satellite record (1998-2015). *Environmental Research Letters*, *14*(12). https://doi.org/10.1088/1748-9326/ab4667

Goris, N., Tjiputra, J. F., Olsen, A., Schwinger, J., Lauvset, S. K., & Jeansson, E. (2018). Constraining projection-based estimates of the future North Atlantic carbon uptake. Journal of Climate, 31(10), 3959–3978. https://doi.org/10.1175/JCLI-D-17-0564.1

Gröger, M., Maier-Reimer, E., Mikolajewicz, U., Moll, A., and Sein, D.: NW European shelf under climate warming: implications for open ocean – shelf exchange, primary production, and carbon absorption, Biogeosciences, 10, 3767–3792, https://doi.org/10.5194/bg-10-3767-2013, 2013

Gutknecht, E., Reffray, G., Mignot, A., Dabrowski, T., & Sotillo, M. G. (2019). Modelling the marine ecosystem of Iberia-Biscay-Ireland (IBI) European waters for CMEMS operational applications. *Ocean Science*, *15*(6), 1489–1516. https://doi.org/10.5194/os-15-1489-2019

Henson, S. A., Dunne, J. P., & Sarmiento, J. L. (2009). Decadal variability in North Atlantic phytoplankton blooms. *Journal of Geophysical Research: Oceans*, *114*(4), 1–11. https://doi.org/10.1029/2008JC005139

Henson, S., Cole, H., Beaulieu, C., & Yool, A. (2013). The impact of global warming on seasonality of ocean primary production. *Biogeosciences*, *10*(6), 4357–4369. https://doi.org/10.5194/bg-10-4357-2013

Henson, S. A., Cole, H. S., Hopkins, J., Martin, A. P., & Yool, A. (2018). Detection of climate change-driven trends in phytoplankton phenology. *Global Change Biology*, *24*(1), e101–e111. https://doi.org/10.1111/gcb.13886

Honjo, S., Eglinton, T. I., Taylor, C. D., Ulmer, K. M., Sievert, S. M., Bracher, A., German, C. R., Edgcomb, V., Francois, R., Deboraiglesias-Rodriguez, M., Van Mooy, B., & Repeta, D. J. (2014). The role of the biological pump in the global carbon cycle understanding an imperative for ocean science. *Oceanography*, *27*(3), 10–16. https://doi.org/10.5670/oceanog.2014.78

Ilyina, T., Six, K. D., Segschneider, J., Maier-Reimer, E., Li, H., & Núñez-Riboni, I. (2013). Global ocean biogeochemistry model HAMOCC: Model architecture and performance as component of the MPI-Earth system model in different CMIP5 experimental realizations. *Journal of Advances in Modeling Earth Systems*, *5*(2), 287–315. https://doi.org/10.1029/2012MS000178

Johnson, K. S., & Bif, M. B. (2021). Constraint on net primary productivity of the global ocean by Argo oxygen measurements. *Nature Geoscience*, *14*(10), 769–774. https://doi.org/10.1038/s41561-021-00807-z

Killick, R., Fearnhead, P., and Eckley, I. A. (2012). Optimal detection of changepoints with a linear computational cost. Journal of the American Statistical Association, 107(500):1590–1598,107(500):1590–1598.

Kulk, G., Platt, T., Dingle, J., Jackson, T., Jönsson, B. F., Bouman, H. A., Babin, M., Brewin, R. J. W., Doblin, M., Estrada, M., Figueiras, F. G., Furuya, K., González-Benítez, N., Gudfinnsson, H. G., Gudmundsson, K., Huang, B., Isada, T., Kovač,

Ž., Lutz, V. A., … Sathyendranath, S. (2020). Primary production, an index of climate change in the ocean: Satellite-based estimates over two decades. *Remote Sensing*, *12*(5), 1–26. https://doi.org/10.3390/rs12050826

Kwiatkowski, L., Aumont, O., Bopp, L., & Ciais, P. (2018). The Impact of Variable Phytoplankton Stoichiometry on Projections of Primary Production, Food Quality, and Carbon Uptake in the Global Ocean. *Global Biogeochemical Cycles*, *32*(4), 516–528. https://doi.org/10.1002/2017GB005799

Kwiatkowski, L., Torres, O., Bopp, L., Aumont, O., Chamberlain, M., Christian, J., Dunne, J., Gehlen, M., Ilyina, T., John, J., Lenton, A., Li, H., Lovenduski, N., Orr, J., Palmieri, J., Schwinger, J., Séférian, R., Stock, C., Tagliabue, A., … Ziehn, T. (2020). Twenty-first century ocean warming, acidification, deoxygenation, and upper ocean nutrient decline from CMIP6 model projections. *Biogeosciences*. 17, 3439–3470. https://bg.copernicus.org/articles/17/3439/2020/

Madec, G. (2015). NEMO ocean engine, Note du Pole de modelisation de l'Institut Pierre-Simon Laplace No 27, ISSN No 1288-1619.

Möllmann, C., Cormon, X., Funk, S. et al. Tipping point realized in cod fishery. Sci Rep 11, 14259 (2021). https://doi.org/10.1038/s41598-021-93843-z

Ramirez-romero, E., Jordà, G., Amores, A., Kay, S., Segura-noguera, M., Macias, D. M., Maynou, F., Sabatés, A., & Alexander, M. A. (2020). *Assessment of the Skill of Coupled Physical – Biogeochemical Models in the NW Mediterranean*. *7*(July), 1–18. https://doi.org/10.3389/fmars.2020.00497

Sanders, R., Henson, S. A., Koski, M., De La Rocha, C. L., Painter, S. C., Poulton, A. J., Riley, J., Salihoglu, B., Visser, A., Yool, A., Bellerby, R., & Martin, A. P. (2014). The Biological Carbon Pump in the North Atlantic. *Progress in Oceanography*, *129*(PB), 200–218. https://doi.org/10.1016/j.pocean.2014.05.005

Seland, Ø., Bentsen, M., Olivié, D., Toniazzo, T., Gjermundsen, A., Graff, L. S., Debernard, J. B., Gupta, A. K., He, Y. C., Kirkeväg, A., Schwinger, J., Tjiputra, J., Schanke Aas, K., Bethke, I., Fan, Y., Griesfeller, J., Grini, A., Guo, C., Ilicak, M., … Schulz, M. (2020). Overview of the Norwegian Earth System Model (NorESM2) and key climate response of CMIP6 DECK, historical, and scenario simulations. In *Geoscientific Model Development* (Vol. 13, Issue 12). https://doi.org/10.5194/gmd-13-6165-2020

https://doi.org/10.5194/bg-2023-54
Preprint. Discussion started: 20 March 2023

Silsbe, G. M., Behrenfeld, M. J., Halsey, K. H., Milligan, A. J., & Westberry, T. K. (2016). The CAFE model: A net production model for global ocean phytoplankton. *Global Biogeochemical Cycles*, *30*(12), 1756–1777. https://doi.org/10.1002/2016GB005521

Six, K. D. and Maier-Reimer, E.: Effects of plankton dynamics on seasonal carbon fluxes in an ocean general circulation model, Global Biogeochem. Cy., 10, 559–583, 1996.

Skyllas, N., Bintanja, R., Buma, A. G. J., Brussaard, C. P. D., Gröger, M., Hieronymus, J., & van de Poll, W. H. (2019). Validation of stratification-driven phytoplankton biomass and nutrient concentrations in the northeast atlantic ocean as simulated by EC-earth. *Geosciences (Switzerland)*, *9*(10). https://doi.org/10.3390/geosciences9100450

Smeed, D. A., Josey, S. A., Beaulieu, C., Johns, W. E., Moat, B. I., Frajka-Williams, E., Rayner, D., Meinen, C. S., Baringer, M. O., Bryden, H. L., & McCarthy, G. D. (2018). The North Atlantic Ocean Is in a State of Reduced Overturning. *Geophysical Research Letters*, *45*(3), 1527–1533. https://doi.org/10.1002/2017GL076350

Smith, B., Wårlind, D., Arneth, A., Hickler, T., Leadley, P., Siltberg, J., and Zaehle, S. (2014). Implications of incorporating N cycling and N limitations on primary production in an individual- based dynamic vegetation model, Biogeosciences, 11, 2027– 2054, https://doi.org/10.5194/bg-11-2027-2014, 2014.

Smyth, T. J., Tilstone, G. H., & Groom, S. B. (2005). Integration of radiative transfer into satellite models of ocean primary production. *Journal of Geophysical Research: Oceans*, *110*(10), 1–11. https://doi.org/10.1029/2004JC002784

Steinacher, M., Joos, F., Frölicher, T. L., Bopp, L., Cadule, P., Cocco, V., Doney, S. C., Gehlen, M., Lindsay, K., Moore, J. K., Schneider, B., & Segschneider, J. (2010). Projected 21st century decrease in marine productivity: A multi-model analysis. *Biogeosciences*, *7*(3), 979–1005. https://doi.org/10.5194/bg-7-979-2010

Sein, D.V, Gröger, M., Cabos, W., Alvarez, F., Hagemann, S., de la Vara, A., Pinto, J.G., Izquierdo, A., Koldunov, N.V., Dvornikov, A. Y., Limareva, N., Martinez, B., Jacob, D. (2020), Regionally coupled atmosphere - ocean - marine biogeochemistry model ROM: 2. Studying the climate change signal in the North Atlantic and Europe J. Adv. Model. Earth Syst., DOI: 10.1029/2019MS001646

Stock, C. A., John, J. G., Rykaczewski, R. R., Asch, R. G., Cheung, W. W. L., Dunne, J. P., Friedland, K. D., Lam, V. W. Y., Sarmiento, J. L., & Watson, R. A. (2017). Reconciling fisheries catch and ocean productivity. *Proceedings of the National Academy of Sciences of the United States of America*, *114*(8), E1441–E1449. https://doi.org/10.1073/pnas.1610238114

Sverdrup, H. U. (1953). On conditions for the vernal blooming of phytoplankton. *ICES Journal of Marine Science*, *18*(3), 287–295. https://doi.org/10.1093/icesjms/18.3.287

Tjiputra, J. F., Schwinger, J., Bentsen, M., L. Morée, A., Gao, S., Bethke, I., Heinze, C., Goris, N., Gupta, A., He, Y. C., Olivié, D., Seland, O., & Schulz, M. (2020). Ocean biogeochemistry in the Norwegian Earth System Model version 2 (NorESM2). *Geoscientific Model Development*, *13*(5), 2393–2431. https://doi.org/10.5194/gmd-13-2393-2020

Truong, C., Oudre, L., & Vayatis, N. (2020). Selective review of offline change point detection methods. *Signal Processing*, *167*. https://doi.org/10.1016/j.sigpro.2019.107299

van Noije, T. P. C., Le Sager, P., Segers, A. J., van Velthoven, P. F. J., Krol, M. C., Hazeleger, W., Williams, A. G., and Chambers, S. D.: Simulation of tropospheric chemistry and aerosols with the climate model EC-Earth, Geosci. Model Dev., 7, 2435–2475, https://doi.org/10.5194/gmd-7-2435-2014, 2014.

Watanabe, K., Seike, K., Kajihara, R., Montani, S., & Kuwae, T. (2019). Relative sea-level change regulates organic carbon accumulation in coastal habitats. *Global Change Biology*, *25*(3), 1063–1077. https://doi.org/10.1111/gcb.14558

Westberry, T., Behrenfeld, M. J., Siegel, D. A., & Boss, E. (2008). Carbon-based primary productivity modeling with vertically resolved photoacclimation. *Global Biogeochemical Cycles*, *22*(2), 1–18. https://doi.org/10.1029/2007GB003078

Yamaguchi, R., Rodgers, K. B., Timmermann, A., Stein, K., Schlunegger, S., Bianchi, D., Dunne, J. P., & Slater, R. D. (2022). Trophic level decoupling drives future changes in phytoplankton bloom phenology. *Nature Climate Change*, *12*(5), 469–476. https://doi.org/10.1038/s41558-022-01353-1

https://doi.org/10.5194/bg-2023-54
Preprint. Discussion started: 20 March 2023

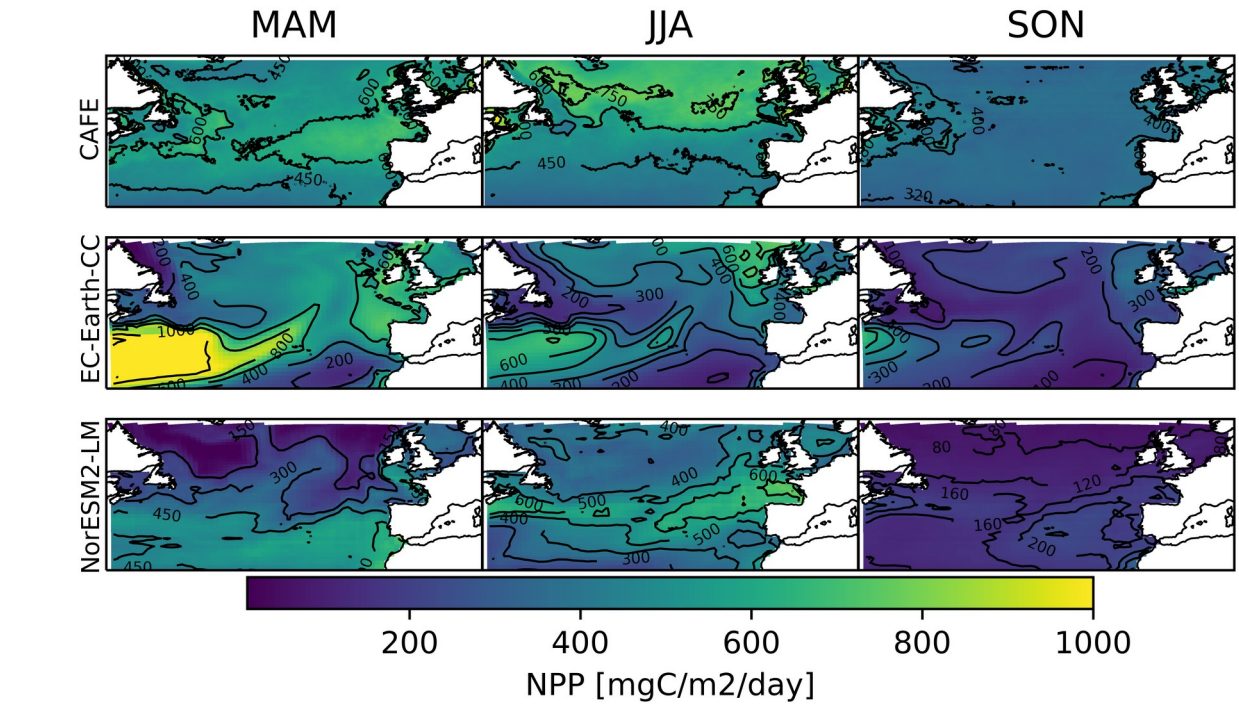

Figure 1: Seasonal mean vertically integrated NPP from the CAFE model (upper), EC-Earth3-CC (middle) and NorESM2-LM (bottom).

https://doi.org/10.5194/bg-2023-54
Preprint. Discussion started: 20 March 2023

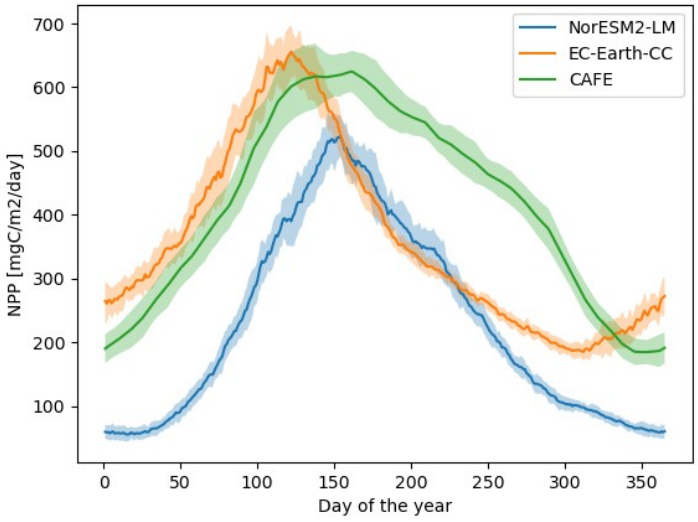

Figure 2: Seasonal cycle of vertically integrated NPP for CAFE, EC-Earth3-CC and NorESM2-LM averaged over 30-60ºN. The model data was masked by the CAFE data to account for the smaller winter domain visible by satellites. A multi-year (2003-2021) average is shown.

https://doi.org/10.5194/bg-2023-54
Preprint. Discussion started: 20 March 2023

Biogeosciences
Discussions
Open Access
EGU

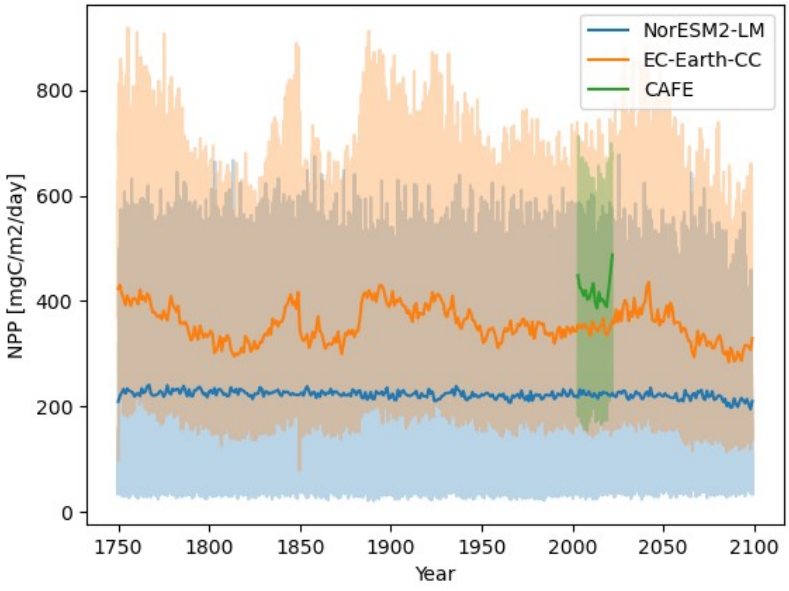

Figure 3: Time-series of annual mean vertically integrated NPP for the different models. Shaded lines display the daily/8 daily ESM/CAFE data.

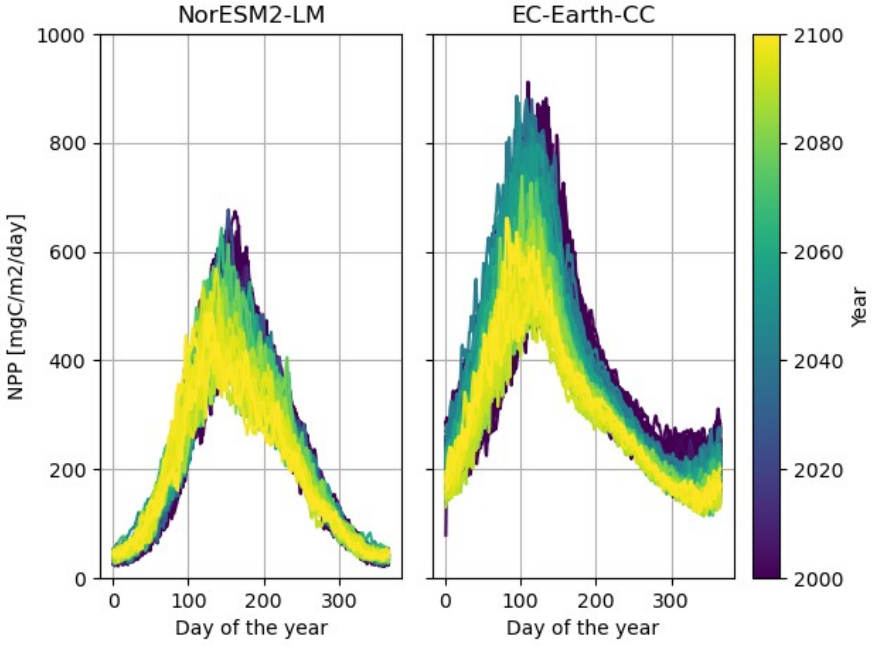

Figure 4: Time-series of vertically integrated NPP for each year from 1850-2100. The years 1850-2000 were plotted in the color of the year 2000 in the colorbar, and the years 2000-2100 were color coded in accordance with the colorbar.

https://doi.org/10.5194/bg-2023-54
Preprint. Discussion started: 20 March 2023

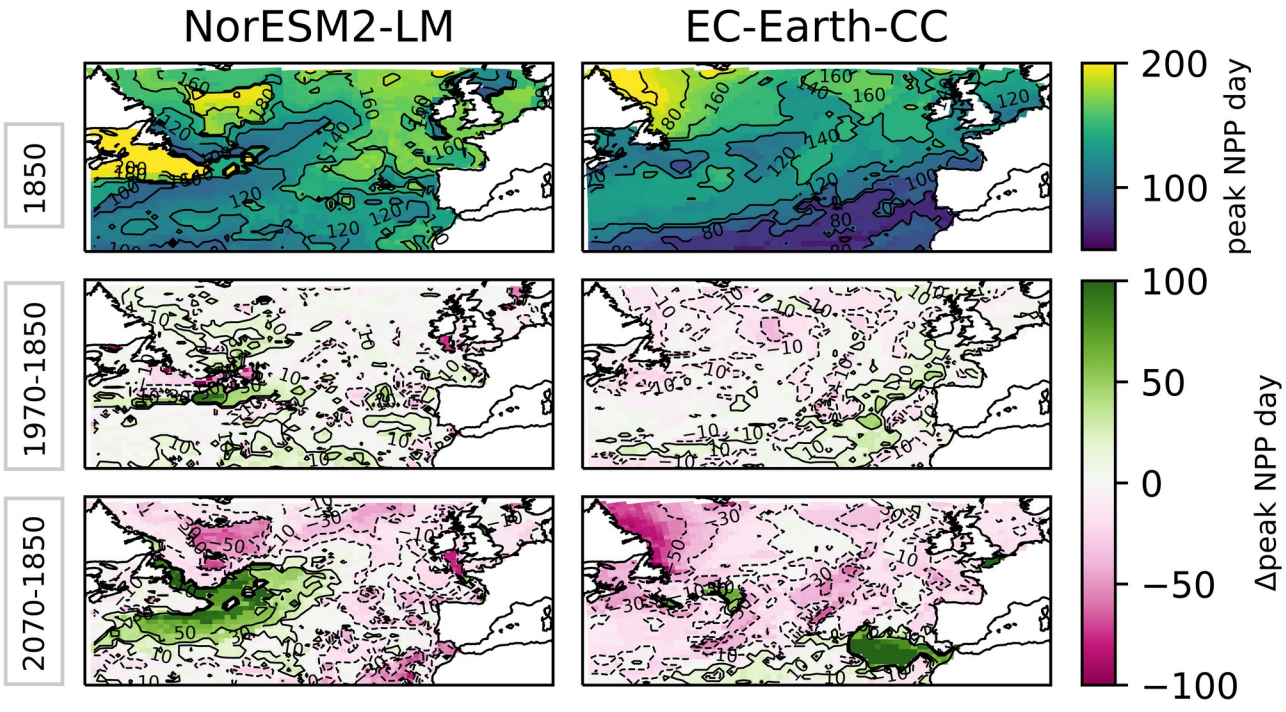

Figure 5: Mean day of peak NPP for NorESM2-LM (left) and EC-Earth3-CC (right) over the years 1850-1879 (top). The bottom panels show mean over 1970-1999 minus the 1850-1879 mean (middle) and the mean over 2070-2099 minus the 1850-1879 mean (bottom).

https://doi.org/10.5194/bg-2023-54
Preprint. Discussion started: 20 March 2023

Biogeosciences Discussions Open Access EGU

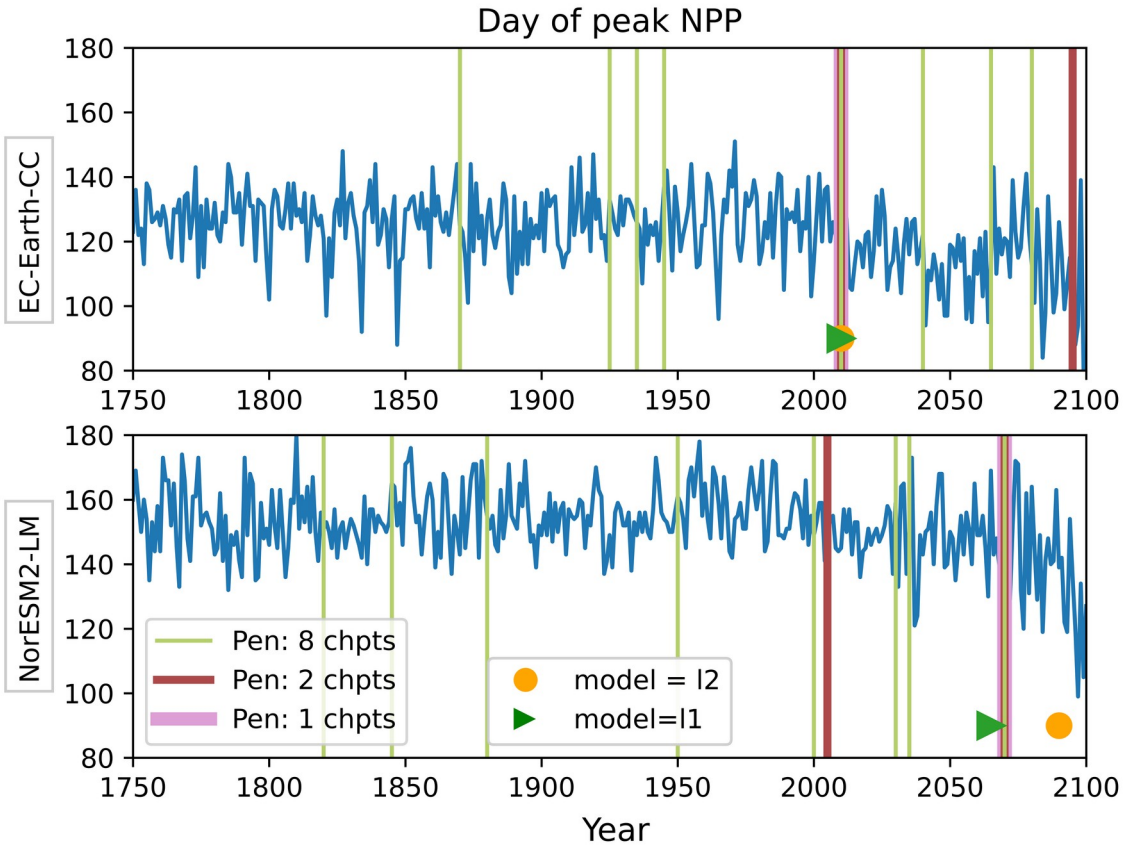

Figure 6: Day of peak NPP for EC-Earth3-CC (top) and NorESM2-LM (bottom). The major change points calculated with a kernel based search method in the time-series are marked by the vertical lines. The different colors represent three different penalties. The pink/red lines correspond to penalties that are tuned to catch one/two change points respectively. The green lines illustrate that a small lowering of the medium penalty generates many more change points in the time series (here tuned to catch eight change points). The different line widths are there so that it is possible to see where the different penalties correspond to the same change points. The orange circle represents the largest change point in the time series that corresponds to a change in the mean (model l2) while the green triangle represents the largest change point corresponding to a change in the median (model l1).

https://doi.org/10.5194/bg-2023-54
Preprint. Discussion started: 20 March 2023

Biogeosciences
Discussions
Open Access
EGU

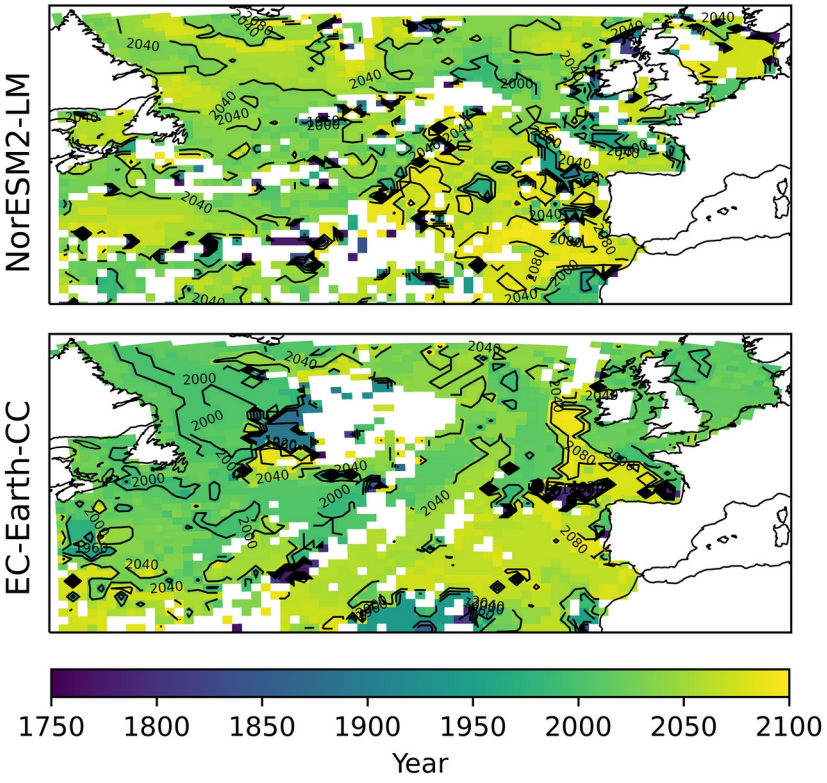

Figure 7: Year of change point of the day of maximum primary production for all grid spaces where a maximum of one change point can be found over the period 1750-2100. White spaces are areas where not only one change point could be found.

https://doi.org/10.5194/bg-2023-54
Preprint. Discussion started: 20 March 2023

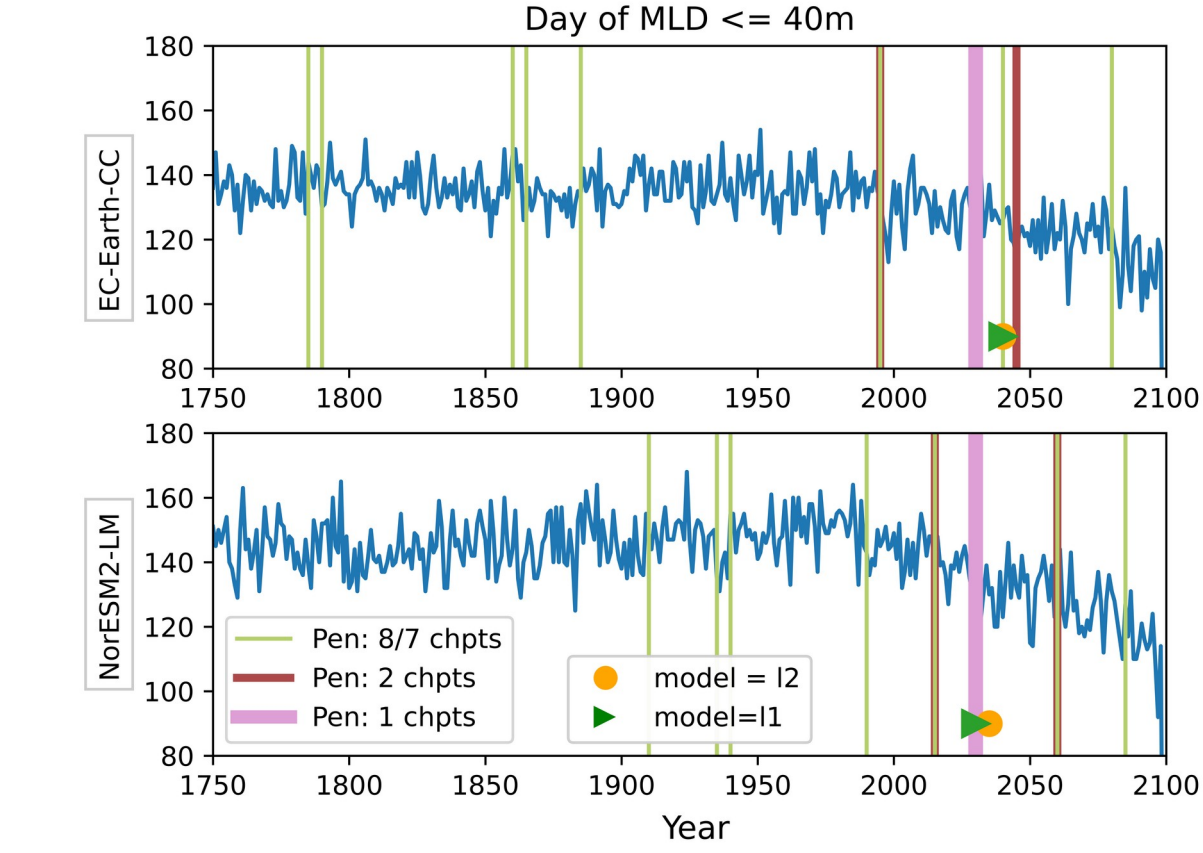

Figure 8: First day of the year when the mixed layer is 40m or less for EC-Earth3-CC (top) and NorESM2-LM (bottom). The major change points calculated with a kernel based search method (rbf) in the time-series are marked by the vertical lines. The different colors represent three different penalties. The pink/red lines correspond to penalties that are tuned to catch one/two change points respectively. The green lines illustrate that a small lowering of the medium penalty generates many more change points in the time series. The different line widths are there so that it is possible to see where the different penalties pick up the same change points. The orange circle represents the largest change point in the time series that corresponds to a change in the mean (model l2) while the green triangle represents the largest change point corresponding to a change

https://doi.org/10.5194/bg-2023-54
Preprint. Discussion started: 20 March 2023

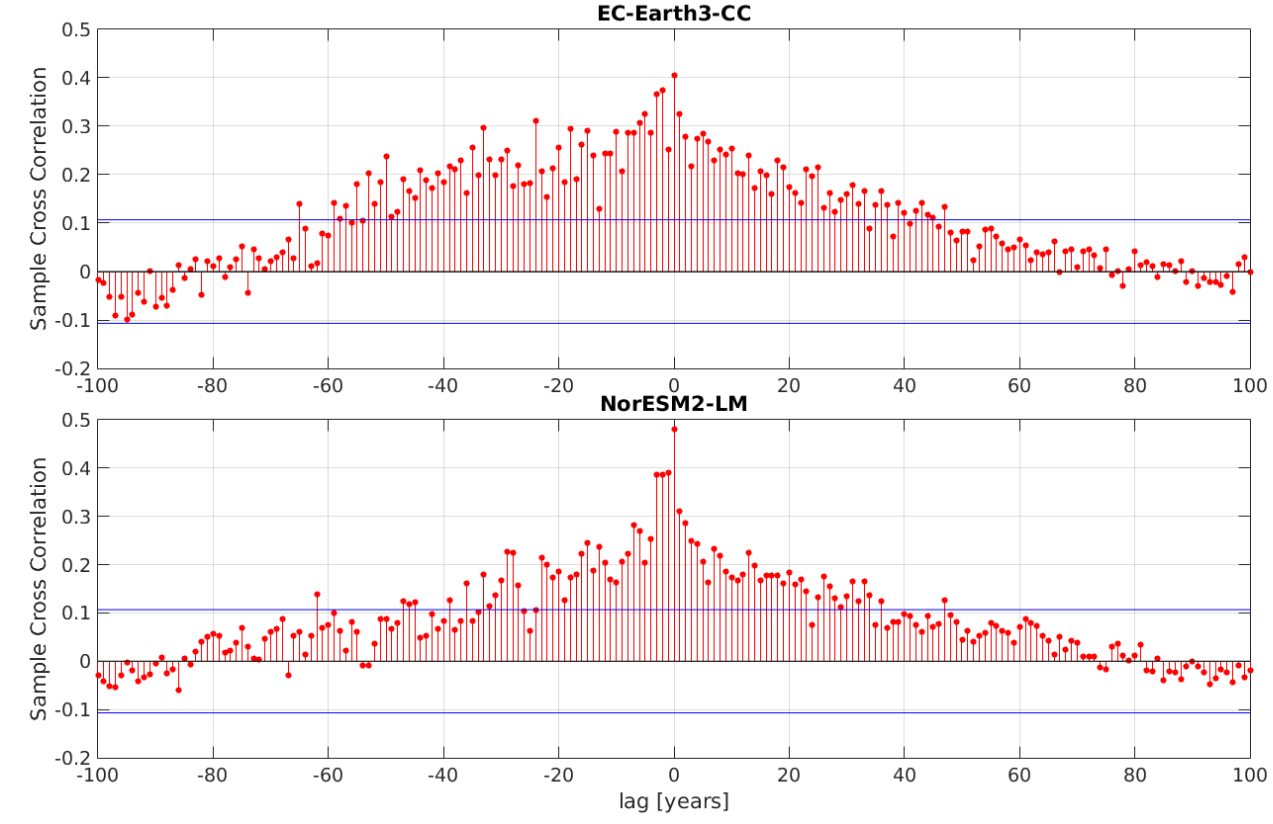

Figure 9: Cross correlation between the day of peak NPP and the first day of mixed layer depth (MLD) smaller than or equal to 40m. Negative lag means that the day of peak NPP proceeds the first day of MLD smaller than 40m, while the opposite holds for positive lag. The horizontal blue lines mark the 95% confidence bounds.